Supporting information

Monometallic Rh Nanocatalyst Supported on CeO_2 Microcuboids for Highly Efficient Dehydrogenation of Hydrous Hydrazine

Wei Wang[#1,2], Shiliang Zhang[#2], Yuanhang Yang[2], Jianhui Xia[*2], Zhang-Hui Lu[*2]

[1]Fujian Key Laboratory of Ecological Impacts and Treatment Technologies for Emerging Contaminants, College of Environmental and Biological Engineering, Putian University, Putian 351100, China

[2]Key Laboratory of Green Catalysis of Jiangxi Education Institutes, College of Chemistry and Materials, Jiangxi Normal University, Nanchang 330022, China

 # These authors contributed equally to this work.

* *Corresponding author: E-mail: xjh2168@126.com; luzh@jxnu.edu.cn*

Materials

Hydrazine hemisulfate salt ($N_2H_4 \cdot 1/2H_2SO_4$, Sigma-Aldrich, 99.5%), *n*-pentane (C_5H_{12}, Sigma-Aldrich, 99.5%), 1,4-dioxane ($C_4H_8O_2$, J&K Chemical, 99.8%), sodium borohydride ($NaBH_4$, J&K Chemical, 98%), hydrazine monohydrate ($N_2H_4 \cdot H_2O$, Sigma-Aldrich, 98%), rhodium chloride trihydrate ($RhCl_3 \cdot xH_2O$, Aladdin, Rh: 38.5-42.5%), cerium nitrate hexahydrate ($Ce(NO_3)_3 \cdot 6H_2O$, J&K Chemical, 99.5%), urea ($CO(NH_2)_2$, Aladdin, ≥99.5%), polyethylene glycol 400 (PEG-400, Tianjin Fuchen Chemical Reagent, 500 mL), polyvinylpyrrolidone (PVP, Sigma-Aldrich, 95%), Sodium hydroxide (NaOH, Tianjin Fuchen Chemical Reagent, ≥96%) were directly used without further purification. Ultrapure water (R=18.3 MΩ cm) was taken as the reaction solvent.

Synthesis of CeO_2 hollow spheres

CeO_2 hollow spheres are prepared using an established route [S1]. Briefly, $Ce(NO_3)_3 \cdot 6H_2O$ (1.0 g) was added to a basic 40 mL mixed solution composed of

different ratios of PEG-400/H_2O with vigorous stirring for 1 h. The mixture was sealed in a 50 mL Teflon-lined autoclave and hydrothermal treatment was conducted at 453 K for 24 h. And then, the solution was filtered, washed several times with distilled water and ethanol in turn, and dried at 353 K for 5 h, which obtained the milky white solid. Afterward, the above sample was transferred to a ceramic crucible and annealed at 773 K for 4 h with the purpose of removing the organic template and trace amounts of impurities in the product. The obtained samples were designated as CeO_2-HS.

Synthesis of CeO_2 octahedrons

CeO_2 octahedrons have been synthesized by a PVP-assisted hydrothermal method according to the previous report [S2]. Typically, 0.121 g of $Ce(NO_3)_3 \cdot 6H_2O$ and 0.062 g of PVP were dissolved in 25.5 mL of de-ionized water and 2.5 mL of anhydrous ethanol under stirring for 30 min at room temperature. The mixed solution was transferred into a 100 mL Teflon-lined autoclave and kept at 473 K for 24 h. After naturally cooled to room temperature, the suspension was centrifuged, washed with distilled water and then dried overnight at 313 K for 12 h, denoted as CeO_2-OC.

Synthesis of CeO_2 cubes

CeO_2 cubes are prepared by a facile NaOH-assisted synthetic method [S3-S4]. In a typical synthetic procedure, $Ce(NO_3)_3 \cdot 6H_2O$ (1.0 g) was dissolved uniformly in 30 mL water. And 10 mL solution containing NaOH (8.0 g) was added into the above solution under vigorous stirring for approximately 10 min. Afterward, the mixed solution was transferred into a 50 mL Teflon-lined autoclave and maintained at 473 K for 24 h. The final sample was obtained by filtration, washed with water, dried and annealed at 623 K for 4 h in a muffle furnace, denoted as CeO_2-CB.

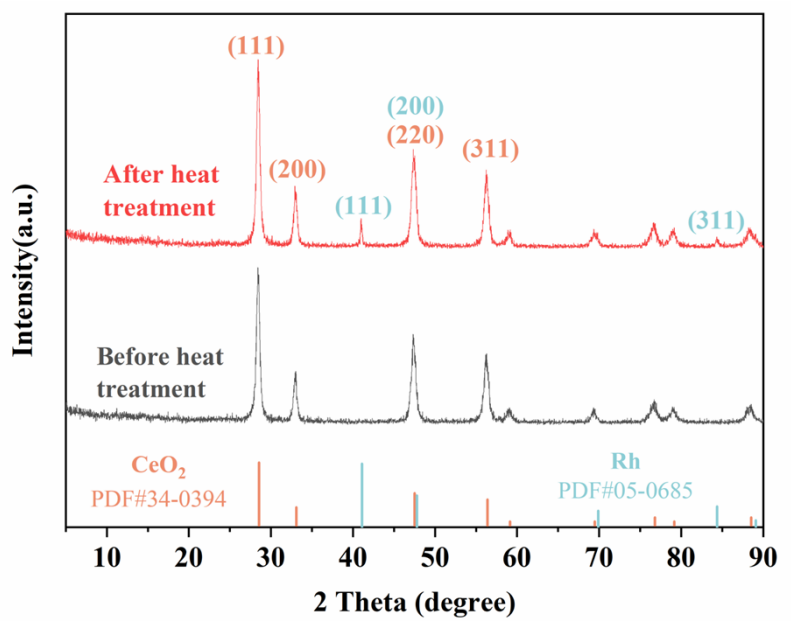

Fig.S1 Powder XRD patterns of Rh/CeO_2-MC catalysts before and after calcination at 823 K for 3 h in an argon atmosphere.

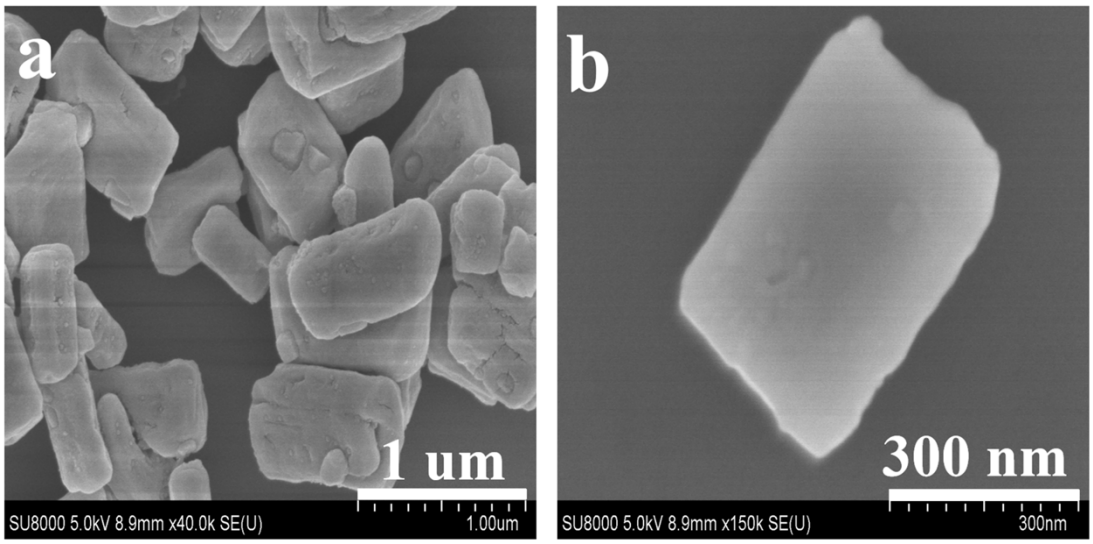

Fig.S2 SEM images of CeO_2-MC.

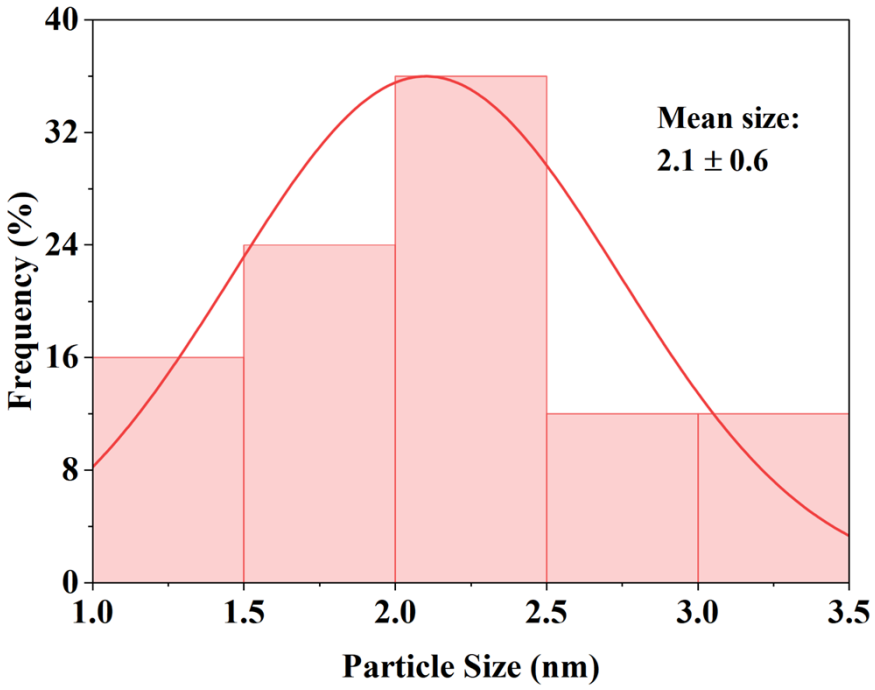

Fig.S3 The particle size distribution diagram of the Rh/CeO_2-MC catalyst was statistically analyzed using the software Nano Measurer.

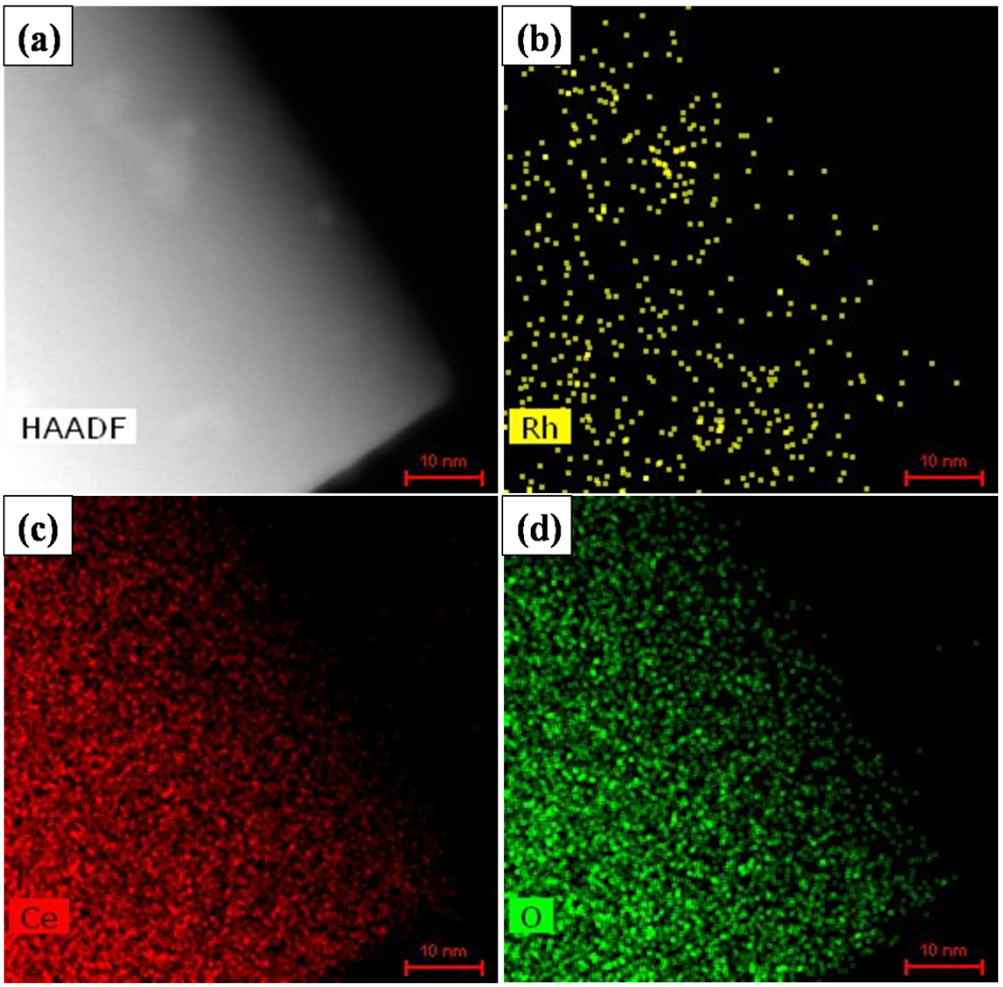

Fig.S4 (a) HAADF-STEM image and (b-d) the corresponding elemental mapping images of Rh/CeO_2-MC catalyst.

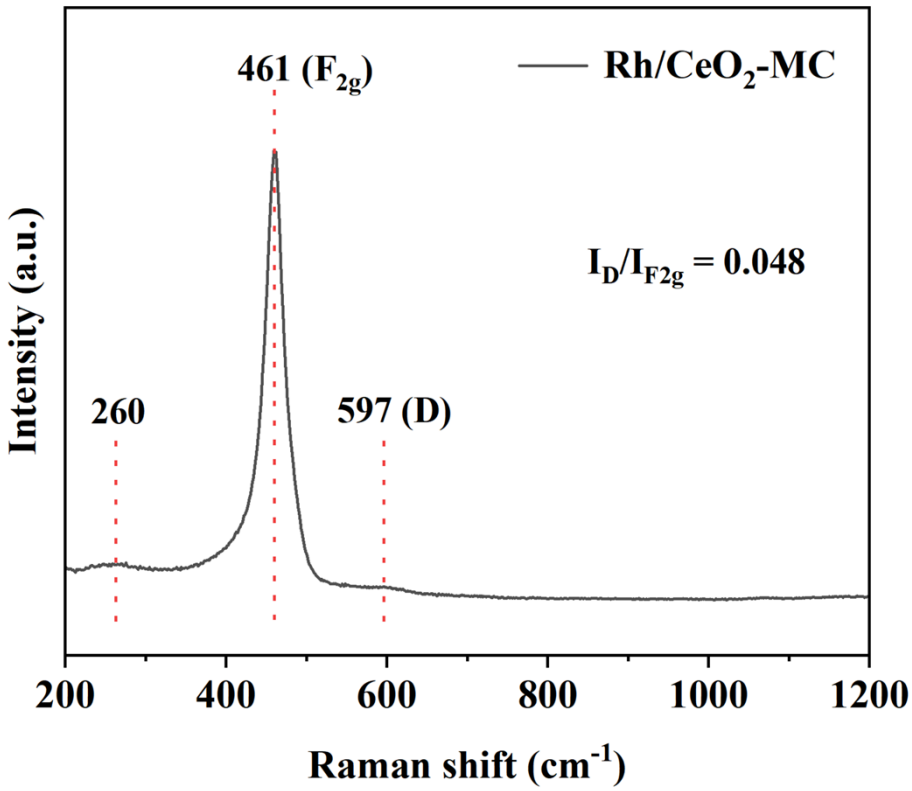

Fig.S5 Raman spectrum and calculated oxygen defect concentration of the Rh/CeO_2-MC catalyst.

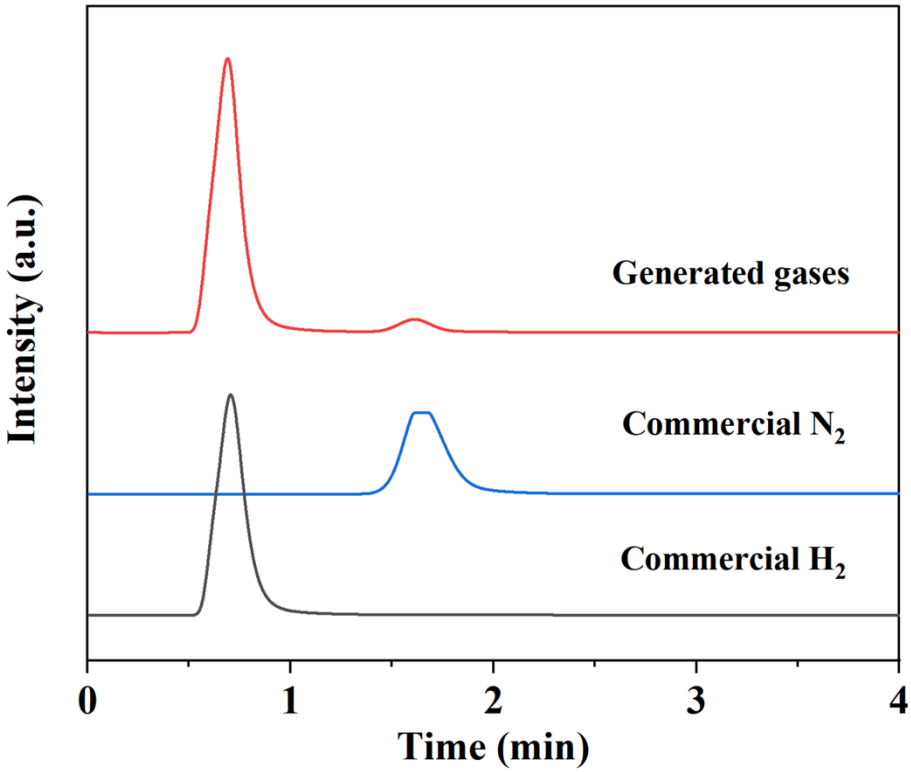

Fig.S6 GC-TCD spectra of commercial H_2, commercial N_2, and generated gases from aqueous N_2H_4 solution catalyzed by Rh/CeO_2-MC.

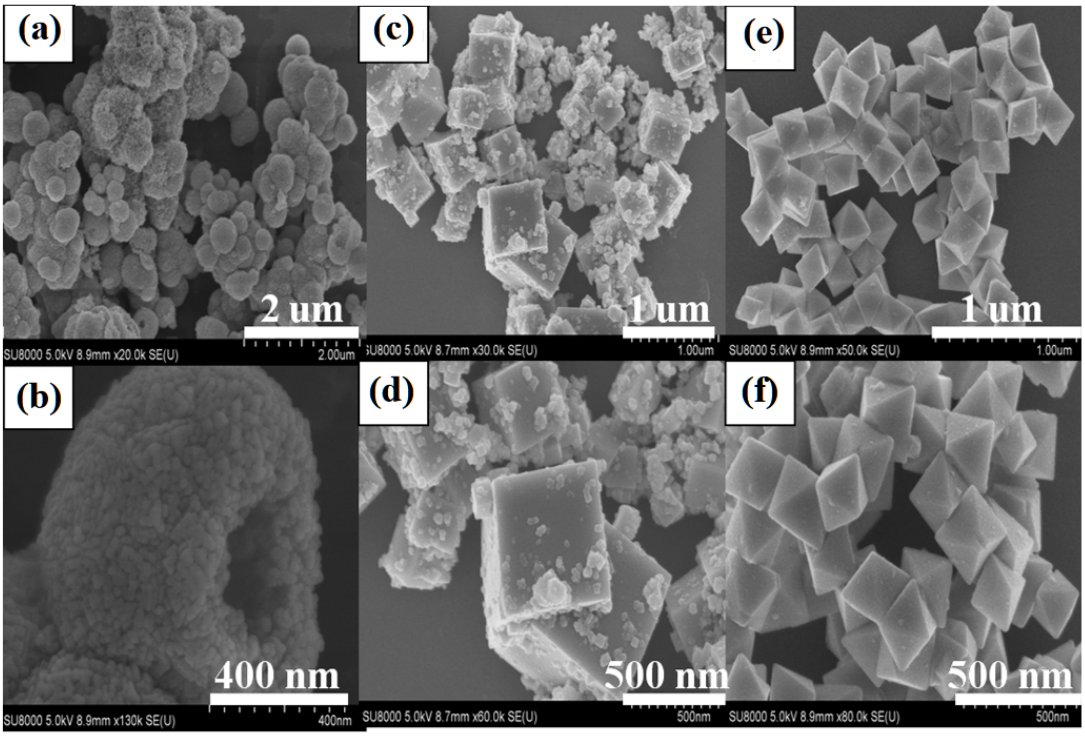

Fig.S7 SEM images of (a,b) CeO_2-HS, (c,d) CeO_2-CB, and (e,f) CeO_2-OC, respectively.

Fig.S8 Typical TEM and high resolution TEM images of (a,b,c) CeO_2-CB, (d,e,f) CeO_2-HS, and (g,h,i) CeO_2-OC, respectively.

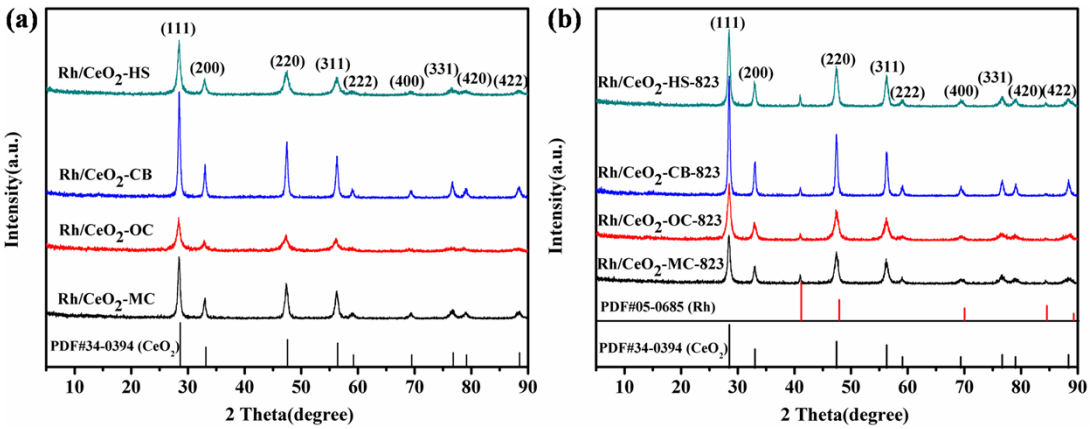

Fig.S9 Powder XRD patterns of (a) a series of Rh/CeO_2 catalysts and (b) a series of Rh/CeO_2 catalysts after calcination at 823 K for 3 h in an argon atmosphere, respectively.

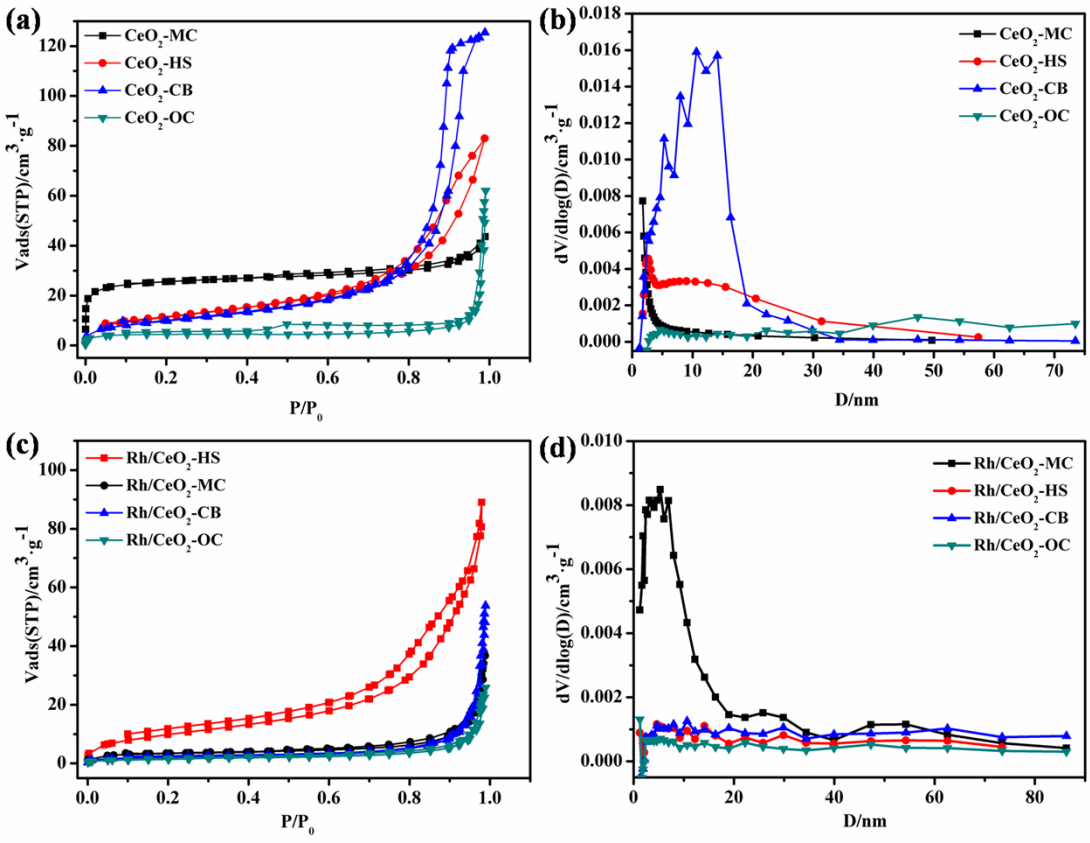

Fig.S10 (a) N_2 adsorption-desorption isotherms and (b) pore size distributions of shape-controlled CeO_2 materials, respectively. (c) N_2 adsorption-desorption isotherms and (d) pore size distributions of Rh/CeO_2-MC, Rh/CeO_2-HS, Rh/CeO_2-CB, and Rh/CeO_2-OC samples, respectively.

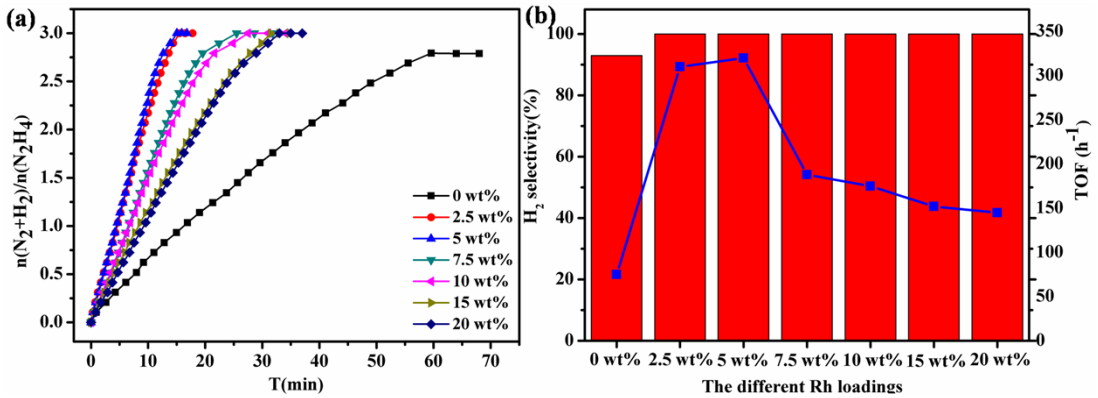

Fig.S11 Time course plot for hydrogen evolution from hydrous hydrazine in the presence of NaOH solution (2.0 M) catalyzed via Rh/CeO_2-MC with the different Rh loadings by changing the dosages of CeO_2-MC samples ($N_2H_4 \cdot H_2O$=0.1 mL, n(Rh)=0.05 mmol, 323 K). (b) The histogram of the corresponding H_2 selectivity and TOF values versus the different Rh loadings.

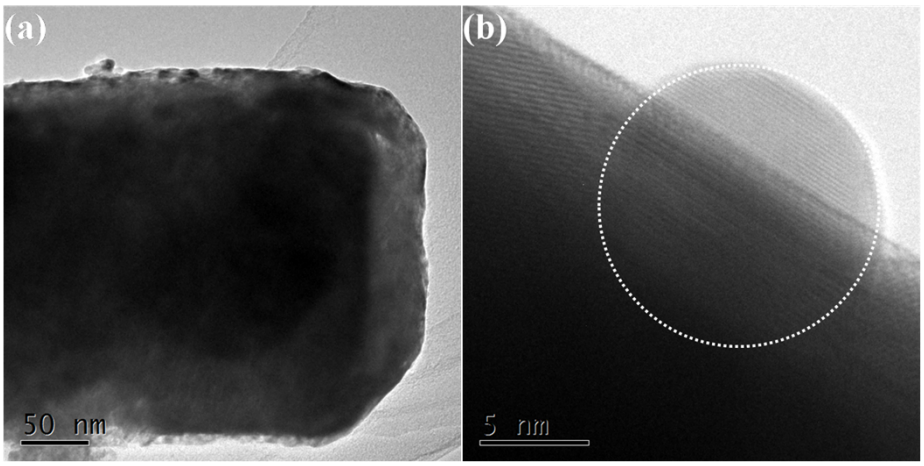

Fig.S12 (a) Typical TEM and (b) high resolution TEM images of Rh/CeO_2-MC catalyst after the durability tests.

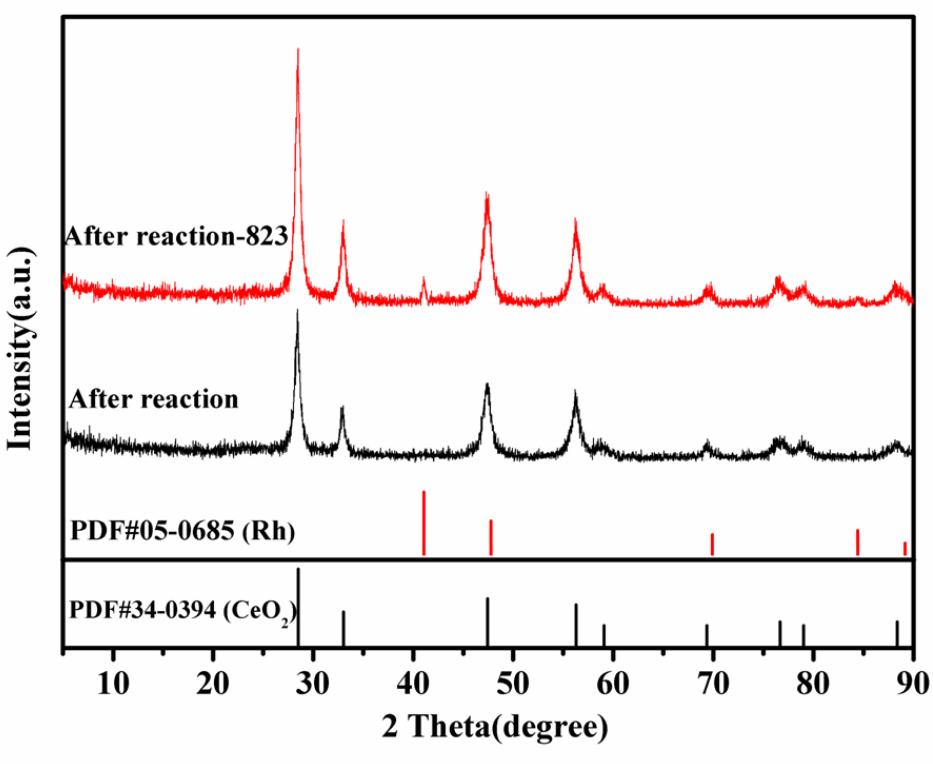

Fig.S13 Powder XRD pattern of Rh/CeO_2-MC catalyst after the durability test and after the durability test followed by further calcination at 823 K for 3 h, respectively.

Calculation method for TOF

The total turnover frequency (TOF) of hydrogen evolution is calculated by the equation (6), wherein n_{H2} is the molar number of hydrogen evolution (mmol), n_{metal} is the molar number of the catalyst (mmol), and t is the reaction time (h).

$$TOF = \frac{n_{H_2}}{\mathrm{n}_{\mathrm{metal}} \times t} \quad \text{(S1)}$$

The TOF values of all the cited catalysts in this work are shown in Table S2 and Table S3 for hydrogen evolution from $N_2H_4{\cdot}H_2O$ and $N_2H_4BH_3$, respectively.

Table S1 Catalytic performances for hydrogen evolution from $N_2H_4 \cdot H_2O$ over some various heterogeneous catalysts.

Catalyst	T (K)	Selectivity (%)	Ea (kJ/mol)	TOF (h^{-1})	Ref.
Cubic Rh_2Ni	293	100	41.6	942	S5
Rh	298	44	-	2.9	33
Rh_4Ni	298	100	-	6.0	S6
RhNi@graphene	298	100	-	20.1	S7
$Ni_{0.9}Pt_{0.1}/Ce_2O_3$	298	100	42.3	27.9	S8
$Rh_{51}Ni_{19}P_{30}$/rGO	298	100	101	58.8	S9
$Rh_{0.8}Ni_{0.2}$@CeOx/rGO	298	100	58.0	36.4	27
RhNiB	303	100	-	54.5	S10
Ni/CeO_2	323	100		34	S11
Ni_3Rh_7/NPC-900	323	100	-	156	36
Rh/CeO_2-MC	323	100	59.3	320	This work
$Rh_{55}Ni_{45}/Ce(OH)CO_3$	323	100	38.8	395	34
$Rh_{0.8}Ni_{0.2}$@MIL-101	323	100	49.8	428.6	35
$Rh_{0.5}(MoO_x)_{0.5}$ NPs	323	100	59.8	750	S12
$Rh_{92.6}P_{7.4}$/rGO	323	100	50.5	843.9	S13

Table S2 BET surface area, pore volume and average pore diameter of all samples.

Sample	S_{BET} (m^2/g)	Pore volume (cm^3/g)	Pore diameter (nm)
CeO_2-OC	15.53	0.091	23.33
Rh/CeO_2-OC	5.73	0.040	27.93
CeO_2-MC	87.29	0.067	3.09
Rh/CeO_2-MC	12.36	0.057	18.39
CeO_2-HS	43.96	0.124	11.25
Rh/CeO_2-HS	33.86	0.131	15.49
CeO_2-CB	36.25	0.194	21.40
Rh/CeO_2-CB	7.80	0.083	42.67

Table S3 Catalytic performances for hydrogen evolution from $N_2H_4 \cdot H_2O$ over Rh/CeO_2-MC, Rh/CeO_2-HS, Rh/CeO_2-CB, and Rh/CeO_2-OC. (Reaction conditions: $N_2H_4 \cdot H_2O$ = 0.1 mL, n(Rh) = 0.05 mmol, Rh loading = 5 wt.%, 323 K, NaOH = 2.0 M).

Catalyst	$n(H_2 + N_2)/n(N_2H_4 \cdot H_2O)$	Time (min)	TOF (h^{-1})	H_2 Selectivity (%)
Rh/CeO_2-MC	3	15.0	320	100
Rh/CeO_2-HS	3	21.5	223	100
Rh/CeO_2-CB	3	26.2	183	100
Rh/CeO_2-OC	3	27.3	173	100

Table S4 Comparison of catalytic activities of some different catalysts for hydrogen evolution from $N_2H_4BH_3$.

Catalysts	T (K)	$n(H_2+N_2)/n(N_2H_4BH_3)$	TOF (h^{-1})	Ref.
$RhCl_3$ pre-catalyst	298	2.93	1200	S14
Rh NPs/HAP	298	3.0	6700	S15
$Ni_{0.9}Pt_{0.1}$-CeO_2	298	5.74	234	S16
$RhCl_3$	323	4.1	-	S17
$Ni_{0.89}Rh_{0.11}$ NPs	323	5.1	9.9	S18
Ni@(Rh_4Ni-alloy)/Al_2O_3	323	5.74	72.0	S19
Rh_4Ni NPs	323	5.8	90	S20
$Ni_{0.9}Pt_{0.1}$/graphene	323	6.0	240	S21
$Rh_{0.8}Ni_{0.2}$@CeOx/rGO	323	6.0	666.7	27
Rh/CeO_2-MC	323	6.0	910	This work
Rh@MgO	323	6.0	2005.3	32
$Ni_{0.9}Pt_{0.1}$@MIL-101	323	6.0	1515	S22

References

[S1] L. J. Han, R. J. Liu, C. S. Li, H. H. Li, C. X. Li, G. J. Zhang and J. N. Yao, Controlled synthesis of double-shelled CeO_2 hollow spheres and enzyme-free electrochemical bio-sensing properties for uric acid, J. Mater. Chem., 2012, 22, 17079-17085.

[S2] Z. G. Wang, W. Z. Bi, S.C . Ma, N. Lv, J. L. Zhang, D. H. Sun and J. Z. Ni, Facet-dependent effect of well-defined CeO_2 nanocrystals on the adsorption and dephosphorylation of phosphorylated molecules, Part. Part. Syst. Charact., 2015, 32, 652-660.

[S3] H. Y. Kim, H. M. Lee and G. Henkelman, CO oxidation mechanism on CeO_2-supported Au nanoparticles, J. Am. Chem. Soc., 2012, 134, 1560-1570.

[S4] H. Y. Tan, J. Wang, S. Z. Yu and K. B. Zhou, Support morphology-dependent catalytic activity of Pd/CeO_2 for formaldehyde oxidation, Environ. Sci. Technol., 2015, 49, 8675-8682.

[S5] C. Li, T. Wang, W. Chu, P. Wu and D. G. Tong, Synthesis of octahedral, truncated octahedral, and cubic Rh_2Ni nanocrystals and their structure-activity relationship for the decomposition of hydrazine in aqueous solution to hydrogen, Nanoscale, 2016, 8, 7043-7055.

[S6] S. K. Singh and Q. Xu, Complete conversion of hydrous hydrazine to hydrogen at room temperature for chemical hydrogen storage, J. Am. Chem. Soc., 2009, 131, 18032-18033.

[S7] J. Wang, X. B. Zhang, Z. L. Wang, L. M. Wang and Y. Zhang, Rhodium-nickel nano-particles grown on graphene as highly efficient catalyst for complete decomposition of hydrous hydrazine at room temperature for chemical hydrogen storage, Energy Environ. Sci., 2012, 5, 6885-6888.

[S8] H. L. Wang, J. M. Yan, Z. L. Wang, Song-Il O and Q. Jiang, Highly efficient hydrogen generation from hydrous hydrazine over amorphous $Ni_{0.9}Pt_{0.1}/Ce_2O_3$ nanocatalyst at room temperature, J. Mater. Chem. A, 2013, 1, 14957-14962.

[S9] X. Q. Du, S. Y. Tan, P. Cai, W. Luo and G. Z. Cheng, A RhNiP/rGO hybrid for efficient catalytic hydrogen generation from alkaline solution of hydrazine, J.

Mater. Chem., A 2016, 4, 14572-14576.

[S10] J. Wang, W. Li, Y. R. Wen, L. Gu and Y. Zhang, Rh-Ni-B Nanoparticles as highly efficient catalysts for hydrogen generation from hydrous hydrazine, Adv. Energy Mater., 2015, 1401879.

[S11] W. Kang and A. Varma, Hydrogen generation from hydrous hydrazine over Ni/CeO_2 catalysts prepared by solution combustion synthesis, Appl. Catal. B-Environ., 2018, 220, 409-416.

[S12] Q. L. Yao, M. He, X. Hong, X. Chen, G. Feng and Z. H. Lu, Hydrogen production via selective dehydrogenation of hydrazine borane and hydrous hydrazine over MoO_x-promoted Rh catalyst, Int. J. Hydrogen Energy, 2019, 44, 28430-28440.

[S13] X. Du, P. Cai, W. Luo and G. Cheng, Facile synthesis of P-doped Rh nanoparticles with superior catalytic activity toward dehydrogenation of hydrous hydrazine, Int. J. Hydrogen Energy, 2017, 695, 3036-3043.

[S14] S. Karahan, M. Zahmakıran and S. Ozkar, Catalytic hydrolysis of hydrazine borane for chemical hydrogen storage: Highly efficient and fast hydrogen generation system at room temperature, Int. J. Hydrogen Energy, 2011, 36, 4958-4966.

[S15] D. Celik, S. Karahan, M. Zahmakırana and S. Ozkar, Hydrogen generation from the hydrolysis of hydrazine-borane catalyzed by rhodium(0) nanoparticles supported on hydroxyapatite, Int. J. Hydrogen Energy, 2012, 37, 5143-5151.

[S16] Z. J. Zhang, Y. Q. Wang, X. S. Chen and Z. H. Lu, Facile synthesis of NiPt-CeO_2 nanocomposite as an efficient catalyst for hydrogen generation from hydrazine borane, J. Power Sources, 2015, 291, 14-19.

[S17] J. Hannauera, U. B. Demirci, C. Geantet, J. M. Herrmann and P. Miele, Transition metal-catalyzed dehydrogenation of hydrazine borane $N_2H_4BH_3$ via the hydrolysis of BH_3 and the decomposition of N_2H_4, Int. J. Hydrogen Energy, 2012, 37, 10758-10767.

[S18] C. Cakanyıldırım, U.B. Demirci, T. Sener, Q. Xu and P. Miele, Nickel-based bimetallic nanocatalysts in high-extent dehydrogenation of hydrazine borane, Int.

J. Hydrogen Energy, 2012, 37, 9722-9729.

[S19] C. M. Li, Y. B. Dou, J. Liu, Y. D. Chen, S. He, M. Wei, D. G. Evans and X. Duan, Synthesis of supported Ni@(RhNi-alloy) nanocomposites as an efficient catalyst towards hydrogen generation from $N_2H_4BH_3$, Chem. Commun, 2013, 49, 9992-9994.

[S20] D. C. Zhong, K. Aranishi, A. K. Singh, U. B. Demirci and Q. Xu, The synergistic effect of Rh-Ni catalysts on the highly-efficient dehydrogenation of aqueous hydrazine borane for chemical hydrogen storage, Chem. Commun., 2012, 48, 11945-11947.

[S21] Z. J. Zhang, Z. H. Lu and X. S. Chen, Ultrafine Ni−Pt alloy nanoparticles grown on graphene as highly efficient catalyst for complete hydrogen generation from hydrazine borane, ACS Sustainable Chem. Eng., 2015, 3, 1255-1261.

[S22] Z. J. Zhang, S. L. Zhang, Q. L. Yao, X. S. Chen and Z. H. Lu, Controlled synthesis of MOF-encapsulated NiPt nanoparticles toward efficient and complete hydrogen evolution from hydrazine borane and hydrazine, Inorg. Chem., 2017, 56, 11938-11945.